J. S. Afr. Inst. Min. Metall., vol. 90, no. 12.
Dec. 1990. pp. 339-344.

Internal power losses occurring at the wavefront of travelling transverse disturbances on mine hoisting cable

by R.R. MANKOWSKI*

SYNOPSIS

The work described here is an extension of current theory applied to obtaining the power dissipated at the wavefront of a transverse disturbance travelling along a mine hoisting cable. A previously derived empirical relation is adapted to the present problem, and is solved by use of a Lagrange-type reference frame moving with the wavefront. As a result of the limitations inherent in the original relation, only a lower-bound for the domain of predicted power losses is defined. A qualitative assessment of conditions leading to the undesirable effects of internal frictional losses at the wavefronts are discussed in terms of the operating environment found on typical mining installations.

SAMEVATTING

Die werk wat hier beskryf word, is 'n uitbreiding van die huidige teorie wat toegepas word om die drywing te bepaal wat gedissipeer word by die golffront van 'n dwarssteuring wat met 'n mynhyskabel langs beweeg. 'n Empiriese verhouding wat vroeër afgelei is, word vir die huidige probleem aangepas en opgelos deur die gebruik van 'n Lagrange-verwysingsraamwerk wat saam met die golffront beweeg. As gevolg van die beperkings wat inherent is aan die oorspronklike verhouding, word slegs 'n anderste grens vir die gebied van voorspelde drywingsverliese gedefinieer. 'n Kwalitatiewe evaluering van die toestande wat tot die ongewenste uitwerkings van interne wrywingsverliese by die golffronte lei, word bespreek in terme van die bedryfsomgewing wat by tipiese mynbou-installasies voorkom.

Introduction

Mechanical engineers observing the winding drums of multi-drum and single-drum winding installations are certain to notice the undesirable resonant conditions occurring on the inclined cable extending from the drum to the headsheave. In these instances of transverse cable vibration, resonant and near-resonant conditions occur when the forcing frequency of the Lebus liner cross-overs approach an integral multiple of the fundamental transverse mode of the inclined cable. Although this cause-and-effect observation is valid for most second-order vibrating systems, the scope of the analytic problem described here is actually fairly broad: depending on the degree of difficulty with which one chooses to quantify the dynamic response of the cable to excitation, an exact mathematical formulation of the problem invariably demands the use of highly nonlinear equations of motion. Often, such attempts lead to intractable systems of equations, with the result that it has become necessary to give increasingly more serious consideration to controlled experimental investigation.

The pioneering efforts of Dimitrious and Whillier[1] and of Harvey[2] in this regard have laid a solid foundation, and given definite direction for research into the vibration of mine hoisting cables. Through their concerned efforts, today's engineers and researchers have been able to pinpoint many of the problems and implement mechanical improvizations where necessary. As a result, the present state-of-the-art of the analysis and theory of cable vibrations is far from static and continues to break fresh ground. In a more recent work, that of Mankowski and Cox[3], the longitudinal attenuation of high-impact stress waves and the degree of penetration and reflection at the cable–drum interface was successfully investigated. In a subsequent experimental investigation[4], an empirical relationship was developed to determine the internal damping characteristics of a mine hoisting cable undergoing large-amplitude nonplanar transverse vibrations in the fundamental and higher harmonic modes.

However, despite the above-mentioned progress, a tantalizing question has persisted through the decades. This centres on the internal losses associated with travelling transverse stress waves. It turns out that, until these losses are fully understood and quantified, further research efforts will continue to fall short of obtaining the exact computer simulation model. This lack motivated the present investigation, in which an attempt is made to shed light on a single aspect of the general problem, namely a quantification of the power loss inherent in a transverse stress wave (pulse) travelling along a mine hoisting cable. In the work described here, the losses are attributed to a Coulomb type of damping mechanism arising from the time-dependent flexure stress cycle travelling with the wavefront. The symbols used are defined at the end of the paper.

Discussion

The fundamental and analytic aspects of the internal damping characteristics of mine hoisting cables as given by Mankowski[4] have a direct bearing in the present investigation. As the present work can be regarded as an extension of that earlier work, the assumptions, nomen-

* Department of Mechanical Engineering, University of Durban–Westville, Private Bag X54001, Durban 4000.

ISSN 0038–223X/3.00 + 0.00. Paper received 8th June, 1990. Modified paper received 28th September, 1990.

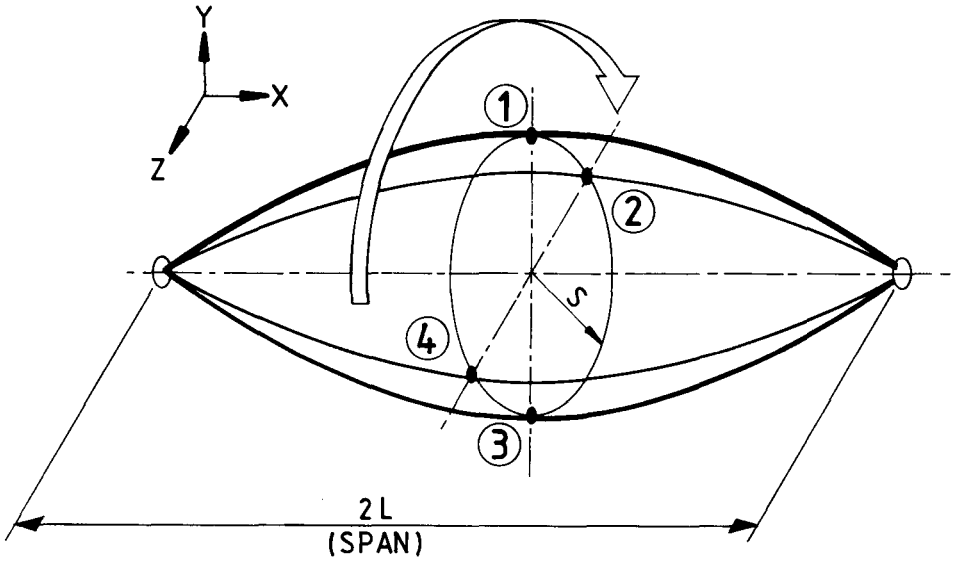

Fig. 1—Envelope of cable undergoing free non-planar transverse vibration in the fundamental mode

clature, and qualitative descriptions are retained here for the sake of continuity. The general empirical relationship derived from experimental evidence is repeated here and given as

$$P(N) = 2N.SSR.F_n.C_1(1,0 + C_2.A_n)\ \text{W}. \quad \ldots\ldots\ldots\ (1)$$

The constants C_1 and C_2 were determined experimentally as 42,75 J and 0,34 m^{-1} respectively, and correspond to a cable of construction $6 \times 30(12/12/6\ TRI)F$ and linear mass density 8,49 kg/m.

The physical parameters for which equation (1) are applicable are shown in Fig. 1, where S is the amplitude of transverse vibration occurring at mid-span.

The boundary conditions in this example are non-rotational, i.e. the cable is constrained in such a manner that it does not rotate about the X-axis. This is better realized in Fig. 2, where a mid-section profile of the cable is shown for the quarter points of one complete cycle. The letter A is assumed physically fixed to the transverse section of the cable. It is noted that the letter A retains its vertical orientation and is seen to revolve about the X-axis. The variation of the flexure stress occurring at the apex of the letter A is also given in this diagram, where the indicators (C –) and (T +) represent the relative states of compressive and tensile stress occurring on the surface of the section indicated as it continues its cycle.

From basic beam theory, the flexure stress on the outermost surfaces of the cable is tensile, while that on the inner surfaces is compressive. The nature of the constraints thus allows the neutral axis, NA, to rotate relative to the cable since, by definition, the neutral axis does not suffer any flexural stress.

Under these boundary conditions, it can be appreciated that all the fibres or individual wires comprising the cable in the span area are sliding cyclically over and against one another. The radial and normal components of flexural (bending) stress are clearly time-dependent and a function of the cable's orientation in space. Likewise, the shear flow, and longitudinal and transverse shearing stress components also depend on the orientation. Moreover, as both of these complementary stresses are dependent on the radius of curvature, R, defined by the relation

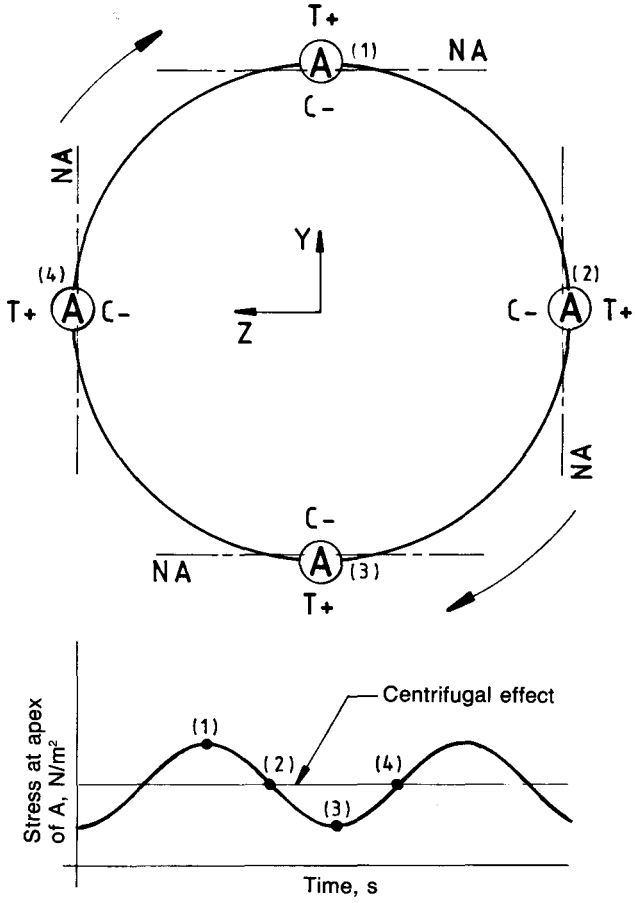

Fig. 2—Flexure stress occurring at a fixed point on the cable, irrotational motion

$$\frac{E}{R} = \frac{M}{I} = \frac{\sigma}{y},$$

the sag-to-span ratio, or dynamically equivalent amplitude-to-span ratio, and the frequency of vibration play an important role in governing the rate of energy loss.

The end result of the energy loss described above can generally be classified as transverse cable fatigue. Fatigue in this instance is manifest by worn individual wires

accompanied by a general loss in their tensile strength as well as ductility.

Internal Losses Occurring at a Wavefront of a Step Pulse

In addition to the above-mentioned energy loss arising from the fundamental and higher harmonic modes or transverse vibration are the local losses associated with the waves of relatively high flexure stress or transverse pulses that are seen originating at the winding drum. These pulses are formed periodically as the cable is forced laterally, and to a lesser extent vertically, through the cross-over areas on the drum. The individual pulses are reflected at the headsheave, and continue to oscillate between the drum and the sheave until the amplitudes and widths are eventually diffused along the inclined cable. As a matter of interest, it is the cumulative effect of the attenuating pulses that eventually set up the standing waves on the inclined cable.

A typical wavefront for a single-step pulse travelling along a cable is shown in Fig. 3, where the configuration depicts two positions of a step pulse spaced $C \cdot dt$ metres apart. Thus, the wavefront lead at L was positioned at L′ dt seconds earlier.

In practice, the flexural rigidity of the cable allows for a continuous and twice differentiable function to fit the trace of the wavefront. A relatively simple mathematical trace that satisfies these requirements and is for all intents and purposes qualitatively correct is given by a trigonometric versine or rotated sine function (Fig. 3), where B is clearly the amplitude of the curved portion measured normal to the gradient LIT in the (X′,Y′) coordinate system. Thus,

$$Y' = B \sin\left(\frac{x' 2\pi \cos(\phi)}{\Omega}\right), \quad 0 \leq x' < \frac{\Omega}{\cos(\phi)}, \quad (2)$$

where $\Omega/\cos(\phi)$ equals the length of the line segment LIT.

Since the slope of the leading portion of the wavefront is zero relative to the coordinates (X, Y), it becomes possible to determine the amplitude B for a given Ω and H. This is accomplished by considering the slope in both coordinate systems:

$$\frac{dY'}{dx'} = \left| B \cos\left(\frac{x' 2\pi \cos(\phi)}{\Omega}\right)\left(\frac{2\pi \cos(\phi)}{\Omega}\right) \right|_{x'y'}$$

$$= \tan(\phi) = \frac{H}{\Omega}\Big|_{xy}. \quad \ldots\ldots\ldots\ldots\ldots\ldots\ldots\ldots\ldots\ldots \quad (3)$$

The evaluation of equation (3) for $x' = 0$ results in

$$B = \frac{H}{2\pi \cos(\phi)} \text{ m}. \quad \ldots\ldots\ldots\ldots\ldots\ldots\ldots\ldots\ldots\ldots \quad (4)$$

Based on the assumption that the slope of any portion of the wavefront does not exceed 90° in the (X,Y) coordinate system (i.e. a vertical slope at the point of inflection at I, Fig. 3), the working or practical range of ϕ will be limited to $0 \leq \phi < 45°$. This limit obviates the existence of a top-heavy wavefront in which a portion of the tail section, IT, is ahead of the leading section, LI, in the direction of travel.

The wavelength Ω is determined by two parameters: the speed of propagation of the transverse pulse C, and the time increment t_p over which the transverse excitation takes place. More precisely, t_p is the duration of time or period that the cable requires to pass through the cross-over arclength as the cable is being wound onto or let out from the winding drum, as the case may be. For a winding drum fitted with a Lebus liner,

$$t_p = \frac{\text{cross-over arclength on drum}}{\text{winding speed of drum}} \text{ s} \quad \ldots\ldots\ldots\ldots \quad (5)$$

$$C = \left(\frac{\text{tension in inclined cable}}{\text{linear mass density}}\right)^{1/2} \text{ m.s}^{-1}. \quad \ldots\ldots\ldots \quad (6)$$

It follows then that

$$\Omega = Ct_p \text{ m}. \quad \ldots\ldots\ldots\ldots\ldots\ldots\ldots\ldots\ldots\ldots\ldots\ldots \quad (7)$$

Equivalence of Losses—Lagrange Coordinate System

The power loss associated with the cable configuration of Fig. 1 is based on a continuous cycle of flexure stress occurring over the complete length of suspended cable and period $(f_n)^{-1}$. Strictly speaking, the nature of the analysis employed in this system uses a Lagrange coordinate system or reference frame in which, after a particular point or particle has been identified, it is 'followed' and the mechanical behaviour is recorded as a function of time. A re-examination of the results shown in Fig. 2 will clarify this point. In this system, a control volume or singular point taken anywhere along the cable (except at the longitudinal centroidal axis) will undergo a complete cycle of flexure stress over the period $(f_n)^{-1}$. The amplitude of the stress variation at these singular points is solely dependent upon their location relative to the rotating neutral axis and, of course, the distance at

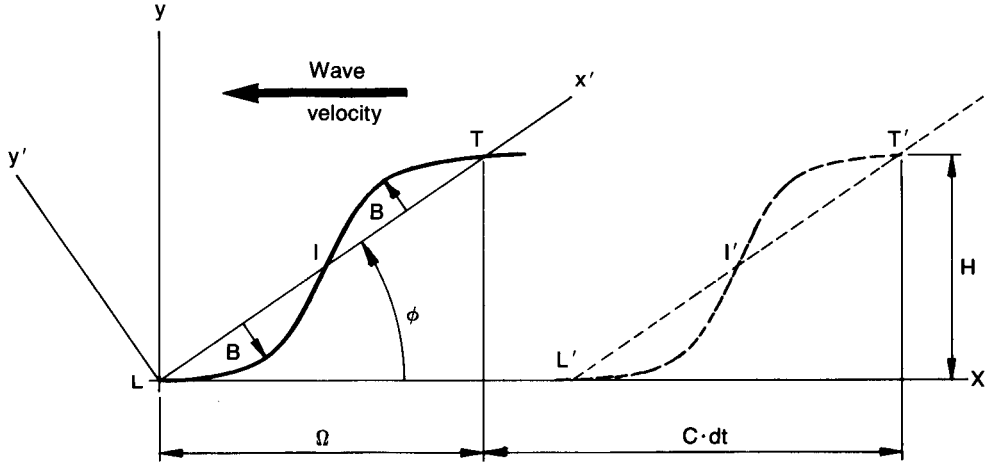

Fig. 3—Geometry of a wavefront
L The front or lead portion of the pulse
T The tail portion of the pulse
I The point of inflection of the wavefront
Ω The wave length of the pulse (m)
C The speed of propagation of a transverse pulse (m/s)
dt A time increment (s)
H The transverse step-amplitude of the pulse (m)

which these points are located from the supports. Clearly, points near the supports will experience a smaller amplitude of stress variation than those situated nearer the centre, where the curvature is higher.

However, in the present analysis the problem is somewhat complicated by the temporal and spatial nature of a left-travelling wave of the general form $G(x + Ct)$. The function G as used here represents the 'rotated' sine function measured relative to the (X,Y) coordinate system, and the argument $(x + Ct)$ indicates the time and position at which the function G is to be evaluated[5]. However, if we again adopt a Lagrange-type reference frame but in this instance fix it to the cable and record the mechanical behaviour of individual points as the stress wave passes through at velocity C, the analytic problem is reduced considerably. In this way, and by considering the collective behaviour of all the individual points entering and leaving the area defined by the wavefront, it becomes possible to use equation (1) to evaluate the power loss expended at the travelling wavefront.

As the mechanical behaviour of the step pulse is measured relative to the cable itself, the translation velocity or winding speed of the drum does not enter the calculations at this point—at least, insofar as the solution to the general wave equation is concerned. Towards this end, the following points are put forward and highlight the loss equivalence between the two systems defined in Figs. 1 and 3.

(1) An arbitrarily fixed point or fibre (except those situated at the non-rotating neutral axis) will experience a complete and single cycle of flexure stress as the wavefront passes through.
(2) The amplitude of the flexure-stress cycle is dependent upon the distance at which the fibres are located from the neutral axis.
(3) The period over which the stress cycle is completed is independent of the position relative to the neutral axis. The frequency of all such cycles is given by $(t_p)^{-1}$ Hz.
(4) The points of maximum curvature occur at the maximum amplitudes of the rotated sine function. In this case, the amplitude is given by B, equation (4).
(5) The equivalent sag-to-span ratio (SSR) occurring at both curved portions of the pulse and taken with reference to the quarter wave length is given by

$$SSR = \frac{2H}{\pi\Omega} = \frac{2\tan(\phi)}{\pi} \text{ (non-dimensional).}$$

Rewriting equation (1) in terms of the above parameters results in an expression for the power dissipated in the interval LIT defined by the wavefront (Fig. 3):

$$P = 2\left(\frac{2H}{\pi\Omega}\right)\left(\frac{1}{t_p}\right)C_1(1{,}0 + BC_2) \text{ W.} \quad \ldots\ldots\ldots\ldots \quad (8)$$

The values C_1 and C_2 of 42,75 J and 0,34 m^{-1} respectively were determined previously and are unique to the experimental cable mentioned earlier. Neglecting the product BC_2 compared with unity introduces an error of less than 1 per cent in the calculation and further reduces the expression to

$$P = \frac{55\tan\phi}{t_p} \text{ W.} \quad \ldots\ldots\ldots\ldots\ldots\ldots\ldots\ldots\ldots \quad (9)$$

Results

A practical range for the excitation period is obtained from the physical parameters of a typical winding installation. For a 180°–180° Lebus liner coiling pattern, the arclength of the coil cross-over area is approximately 0,45 m, while the winding speeds can vary anywhere from 15,0 $m.s^{-1}$ upwards to 20,0 $m.s^{-1}$. Thus, from equation (5),

$$0{,}020 \leq t_p \leq 0{,}030 \text{ s.}$$

The general slope of the wavefront, defined by $\tan(\phi)$, is solely a function of the step amplitude, H, and of Ω, the width of the pulse, equation (7). Recall that, for practical limitations, the range of ϕ was confined to the interval

$$0{,}0 \leq \phi < 45{,}0 \text{ degrees.}$$

A plot of equation (9), Fig. 4, depicts a family of curves generated by varying ϕ and t_p within the ranges described above. Two points of interest are immediately noticeable and refer to the general trend shown.

(a) The steeper the gradient of the wavefront, the higher the internal power losses.
(b) The faster the winding speed, the higher the internal losses.

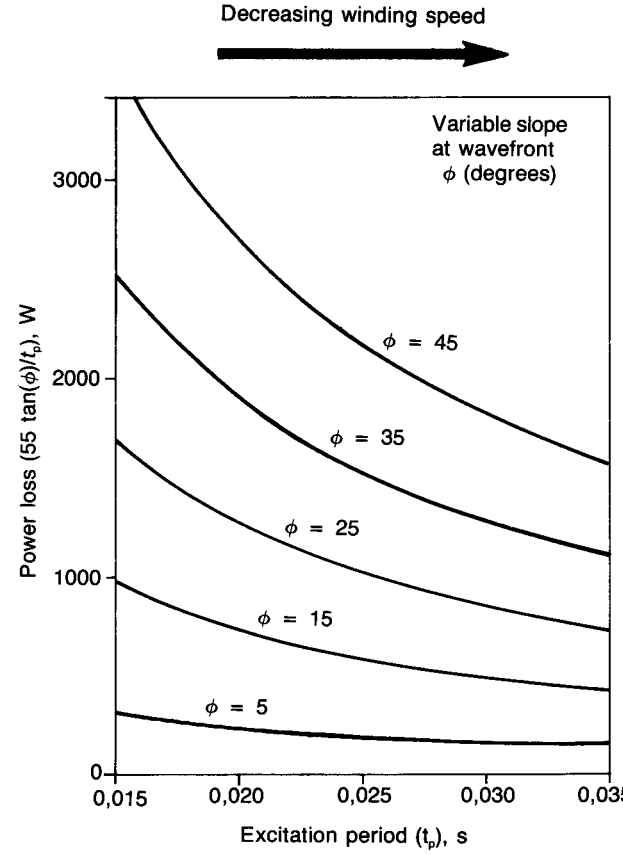

Fig. 4—Effect of increasing slope on internal power loss

At this point it can be correctly argued that points (a) and (b) describe one and the same condition since $\tan(\phi)$ is defined by H and Ω. However, it may not be immediately obvious that the power losses are coupled to the magnitude of the suspended load or conveyance *and* the

position of the conveyance in the vertical shaft. To clarify this point, equation (9) is rewritten here in a form in which the step amplitude, H, is set at a nominal value of ten cable diameters, say 0,45 m, as

$$P = \frac{25}{C(t_p)^2} \text{ W.} \quad \ldots\ldots\ldots\ldots\ldots\ldots\ldots\ldots\ldots\ldots \quad (10)$$

A plot of equation 10 (Fig. 5) now reflects the effect of varying the speed of propagation on the internal power loss at the wavefronts. A third point of interest is drawn here based on the dependence of C on the tension in the inclined cable, equation (6).

(c) An increase in depth of wind requires more cable to be suspended in the vertical shaft, with the result that C will increase accordingly. The effect of higher tension (other variables being fixed) is thus to decrease the power loss at the wavefront. It follows also that an empty conveyance or skip causes a proportionally higher power loss than a fully loaded one.

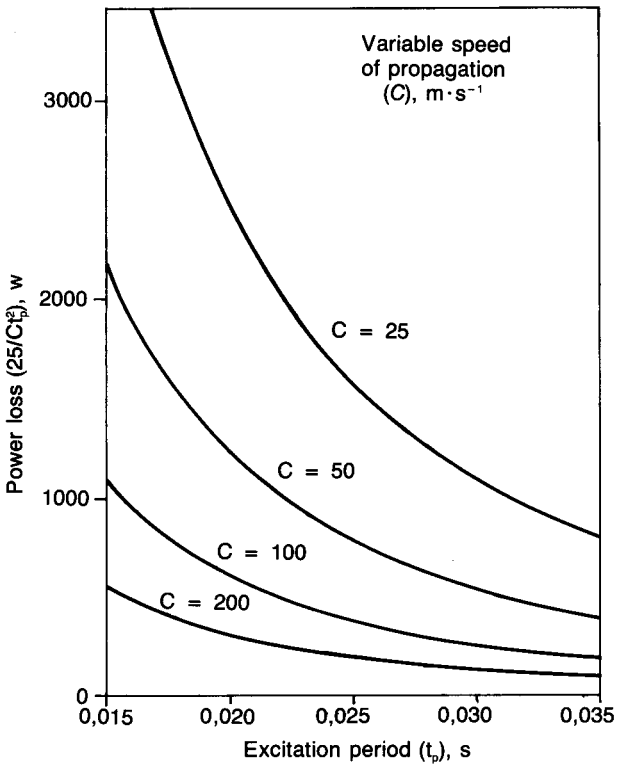

Fig. 5—Effect of increasing tension on internal power loss

The three points above naturally lead to a qualitative description of the most undesirable set of conditions leading to power loss and subsequent fatigue damage at the wavefront. While overall resonant conditions in the inclined cable are known[6], to hasten the onset of fatigue damage and shorten the working life of the cables themselves, the results presented here indicate that (in addition to resonant conditions) the isolated effect of periodic low tension can be identified as one of the major contributing factors reducing the life expectancy of mine-hoist cables. Fig. 5 to a large extent substantiates this point. One condition that is conducive to periodic low tension occurs during the reflection and transmission of step pulses at the boundaries of the inclined cable. Another condition occurs when, if the inclined cable is vibrating in what is commonly known as the planar 'whipping' mode (Mankowski and Whillier[7]), the tension periodically falls to values approaching zero, with the result that concomitant slack conditions at the wavefront are set up.

Limitations of the Present Mathematical Model

It must be pointed out that the relation of internal power loss given by equations (9) and (10) in their present form represents a lower-bound for the predicted power loss for a given set of geometrical and dynamic conditions at the wavefront. In the derivation of equation (1), a critical radius of curvature was evident in the experimental data used to determine the range of acceptable inputs for which the domain of the predicted power losses was valid. It turned out in that investigation that, for radii with a curvature of less than 43 m, the power loss was governed by a nonlinear exponential function. As yet, the precise form of that function is not known, particularly the values of the constants C_1 and C_2. It is expected that, for radii of curvature within this range, these constants will lose their independent character and be expressed as nonlinear functions of *SRR* and frequency. For radii of curvature greater than 43 m, the losses were found to be directly proportional to these variables as indicated by the linear relationship in equation (1). A simple calculation based on the geometrical limitations of the present model shows the radii of curvature to lie in an interval of 5 to 20 m. As a result of the author's familiarity with the apparatus used in deriving equation (1) and subsequent experience in preparing the graphical displays, it is felt that the ordinate values of the power loss indicated in the diagrams of the present paper are at least two to three times larger than shown. While this assessment may appear quantitatively unacceptable, it nevertheless is based on a very conservative and guarded estimate. Moreover, and perhaps more important, the fundamental observations made in the three points above remain qualitatively correct since these losses are based on a monotonically increasing and linear function of *SSR* and f_n.

Conclusion

Current linear theory used to describe the internal power loss inherent in large-amplitude transverse vibrations of mine hoisting cables was applied to the geometric and dynamic properties associated with a travelling transverse wavefront. The main obstacle in achieving a quantitatively correct prediction of these power losses is the lack of precise knowledge of the damping capacity, C_1, and curvature characteristic, C_2, for cables having radii of curvature less than 43 m. However, the results obtained do define a base line or minimal expected power loss for a given set of dynamic conditions in typical mining installations. It should be emphasized that, while the following conclusions are based on the dynamic response of a single mine-hoist cable of fixed construction, the nature of the analysis and subsequent observations given in this paper allow for a general qualitative identification of parameters leading to the detrimental effects associated with fatigue damage at wavefronts.

(1) The gradient of a wavefront has a direct bearing on the internal power loss. Steep fronts cause high periodic flexure stress, which in turn increases frictional losses.
(2) The gradient of a wavefront is determined by three independent parameters: the speed of propagation of transverse pulses, the duration of time the pulse is formed in the coil cross-overs on the drum surface, and the amplitude of the step pulse.
(3) As the speed of propagation of transverse waves increases with an increase in tension, the position of the skip in the vertical shaft and the weight of the payload have a direct bearing on the power losses at the wavefronts.
(4) High winding speeds are detrimental in the sense that the width of a pulse (and hence the gradient) is governed by the period of excitation as the cable passes through the coil cross-overs.
(5) For typical mine installations, a worst possible case based on the four points above occurs when a descending empty skip near the surface is travelling at maximum velocity. This case is further exacerbated if the inclined cable is experiencing a planar 'whipping' mode during which the tension periodically approaches dangerously low levels.

Accepting that the base-line power losses are about two to three times higher than predicted in the foregoing example, it would appear that one aspect of future research could well be directed to a re-examination of the geometry of the popular Lebus liner installed on the majority of South African mines. Such efforts could be undertaken with the sole view of increasing the coil cross-over period, t_p. As cable fatigue is a cumulative and irreversible phenomenon occurring over 75 000 trips per cable (and hundreds of thousands of passes through the coil cross-overs), there is little doubt that such efforts would have positive and practical implications for the mining industry.

Proposal for Future Research

The investigation described here attempted to identify the major parameters leading to the undesirable effects arising from steep gradients at transverse wavefronts. At this point, mining engineers may well ask, 'Fine, but what are the physical effects of the transverse power losses on expected rope life and load-carrying capacity? How can we optimize the design parameters to minimize the deteriorating effect of this phenomenon?'

The need for answers to these two queries is the prime motivating factor leading to continued research efforts into transverse fatigue damage and its concomitant expected rope life. In this regard, it appears that the understanding and quantification of the cause and effects of transverse fatigue damage are, unfortunately, still in their infancy.

Research planning is under way to address this problem. In short, the construction and commissioning of laboratory models to tie-up the relationships among transverse fatigue limits, load-carrying capacity, and safety factors represent the main thrust of ongoing research in this area.

Acknowledgements

The major catalyst in initiating the present investigation was the material extracted from an analysis of film footage taken from Kloof Gold Mine and Winkelhaak Coal Mine during the mid-1970s. A special note of gratitude is recorded here to the mining engineers at those mines who enthusiastically gave of their time in hosting the frequent visits of the research team from the Chamber of Mines Research Organization (COMRO) during those years. The late Dr Austin Whillier, former Head of Vibrations Research at COMRO, was this author's chief mentor in that team. His high standards and professional contributions to the engineering fraternity continue to inspire scores of research efforts across a wide variety of engineering disciplines. It is appropriate that this paper be dedicated to his memory.

List of Symbols

A_n Amplitude of vibration (m)
C_1 Damping capacity (J)
C_2 Curvature characteristic (m^{-1})
E Young's modulus ($N.m^{-2}$)
F_n Frequency of vibration (Hz)
I Moment of inertia (m^4)
M Moment (N-m)
n Mode or harmonic number
$P(n)$ Internal power loss for the n^{th} mode (W)
R Radius of curvature (m)
Span Straight-line distance between supports of vibrating suspended cable (m)
SSR Sag-to-span ratio. (For the fundamental and higher harmonic modes, SSR is defined as the ratio of the amplitude to the quarter-wave length (span/2n) of the standing wave set up on the cable.) Thus,

$$SSR = 2n \cdot A_n/\text{span}$$

Y Distance from neutral axis (m) solids

References

1. DIMITRIOUS, C., and WHILLIER, A. Vibration in winding ropes: An appraisal. Johannesburg, Chamber of Mines Research Laboratories, internal report, Project no. 105/71. Sep. 1973.
2. HARVEY, T. Escort—a winder braking system. *S. Afr. Inst. Elec. Eng.*, vol. 56, Pt 2. 1965. pp. 37–57.
3. MANKOWSKI, R.R., and COX, F.J. Response of mine hoisting cables to longitudinal shock load. *J. S. Afr. Inst. Min. Metall.*, vol. 86, no. 2. Feb. 1986. pp. 51–60.
4. MANKOWSKI, R.R. Internal damping characteristics of a mine hoist cable undergoing non-planar transverse vibration. *J. S. Afr. Inst. Min. Metall.*, vol. 88, no. 12. Dec. 1988. pp. 401–410.
5. CANNON, R.H. *Dynamics of physical systems.* New York, McGraw-Hill. 1967. pp. 465–467.
6. MANKOWSKI, R.R. A study of nonlinear vibrations occurring in mine hoist cables. PhD thesis, University of the Witwatersrand, Johannesburg, 1982.
7. MANKOWSKI, R.R., and WHILLIER, A. Whip in hoist ropes. Chamber of Mines Research Laboratories, internal report. Project no. 105/71, research report 28/74.

Technical note

The production of soda ash at Sua

by B.A. BEEMING*

The soda ash project at Sua has been designed to produce 300 kt per year of soda ash and 600 kt per year of salt from the brines of the Magadikgadi Depression. The capital cost, including the soda ash terminal facilities in the Transvaal, will be R920 million, and the project will be commissioned by April 1991; construction started in November 1988.

The plant will employ some 550 people; during the construction, the site staff and labour peaked at 2800.

Apart from the brine extracted from the pan, the major raw material used is coal, obtained from Maropula Colliery. A simplified flow sheet is shown in Fig. 1, and the layout of the project in Fig. 2.

The brine is extracted from 56 wells at 2 km centres at a rate of up to 2200 m^3/h, and is pumped via a mild-steel line to solar ponds. Corrosion is not a major problem since the brine has a pH of 9,4 and the plant is sited in an arid area.

The brine entering the solar ponds is stored in a shallow pond, average depth 100 mm, where it cools by radiation overnight. The brine is transferred when cold in the early morning (23°C in summer and 8°C in winter) to a 2 m deep pond to provide cooling water for the plant. The brine passes to a 7 km^2 concentrating pond, in which it evaporates until it reaches saturation. The saturated brine is then transferred to the crystallizing ponds, in which salt crystallizes and the brine is concentrated further until it contains some 5 per cent Na_2CO_3, at which point losses of carbonate as trona ($Na_2CO_2.NaHCO_3.2H_2O$) become excessive. The salt crystallizers are taken out of operation in rotation and drained, and the salt is harvested mechanically and transported to a wash plant by tractor trailer. The concentrated brine is pumped to the process plant via a storage pond of 72 days capacity.

Soda ash is recovered from the brine by the conversion of the relatively soluble sodium carbonate to less soluble sodium bicarbonate through reaction with carbon dioxide. The bicarbonate is recovered by thickening followed by filtration. Belt filters were selected to permit complete removal of the mother liquor by efficient countercurrent washing. The bicarbonate is converted back to carbonate by being heated in a steam-tube rotary kiln, from which the carbon dioxide evolved is recovered and returned to the carbonator. Losses of carbon dioxide are made good by carbon dioxide recovered from boiler flue gas in a mono-ethanolamine absorption system.

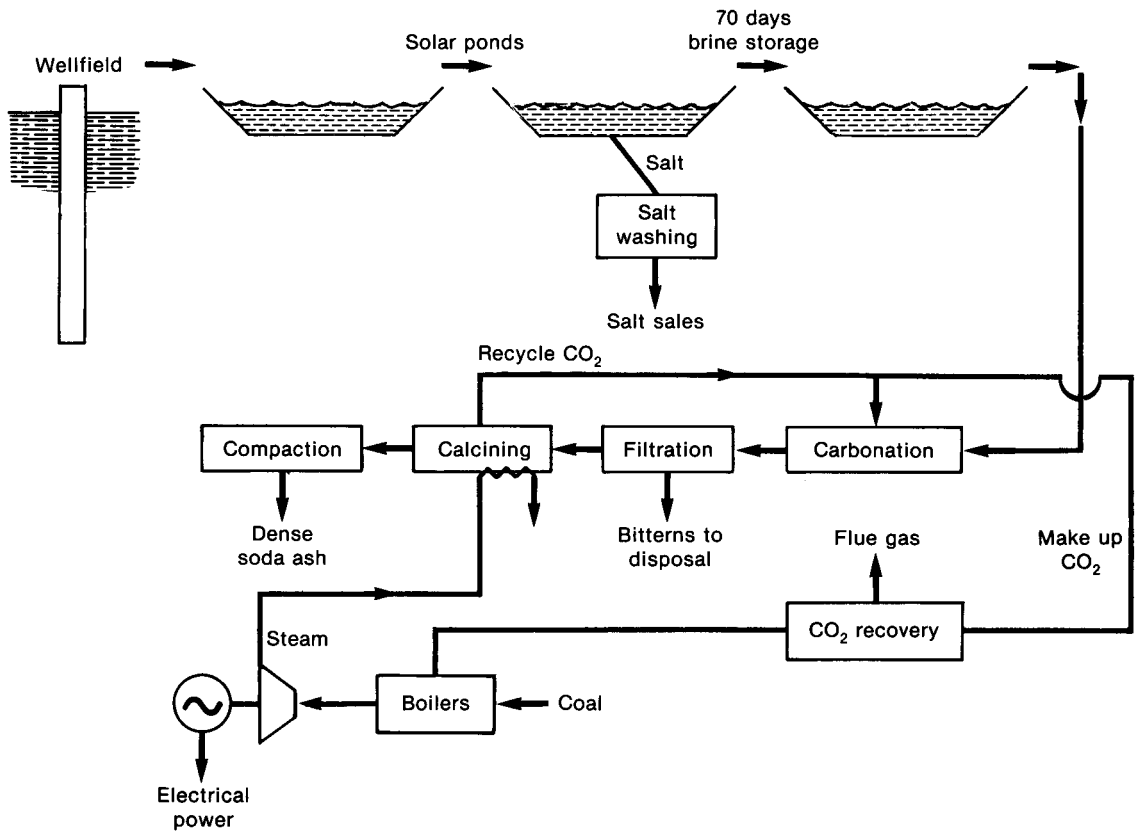

Fig. 1—Simplified process flow diagram

* Soda Ash Botswana (Pty) Ltd, Private Bag 00111, Gabarone, Botswana.

The soda ash produced from the kilns is too fine for commercial use, and is compacted into solid sheets, which are milled and screened to produce the desired product.

Steam is generated in two Babcock 85 t/h 65-bar fluidized-bed boilers. The steam for process use at 20 bars and 2 bars is let down through a 20 MW turbo-alternator producing the power required by the plant.

The residual brine, after the carbonate has been extracted, is evaporated to dryness in a 10 km^2 pond to prevent the brine being recycled to the resource. The level of this bitterns-pond system will not exceed 3 m to avoid visual disturbance to the area.

The project, being sited in a very remote area, required substantial infrastructural services, including an access road, a branch line to the rail head at Francistown (175 km), a potable water supply, and a village.

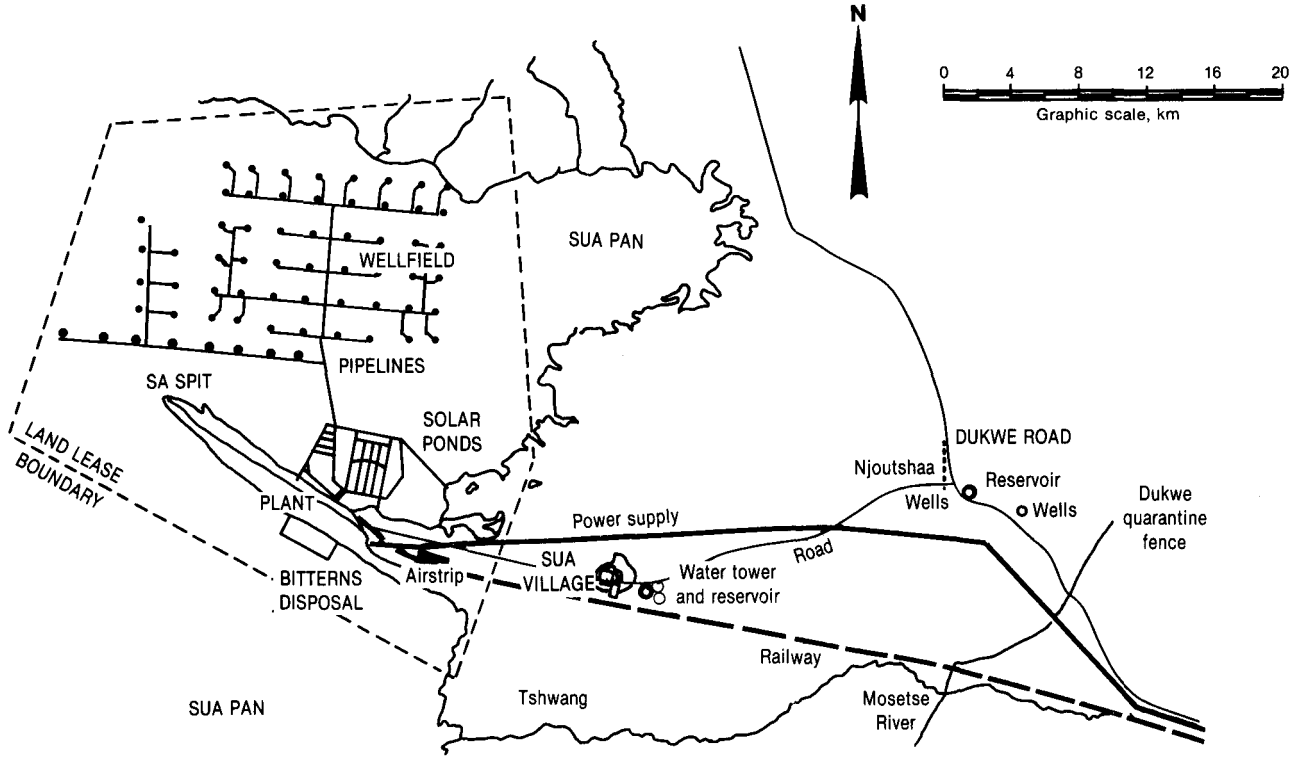

Fig. 2—Layout of pan, wellfield, and infrastructure

Acid mine drainage*

South African coal, gold, and base-metal mines will have to equip themselves with the expertise to manage acid mine water effectively, or risk suffering the same fate as some mines in Canada that will have to spend almost a quarter of their entire profits for the next two decades on combating this problem.

This emerged during a recent two-day course on acid mine drainage (AMD) in Sandton, co-presented by the engineering consulting firm of Steffen, Robertson & Kirsten (SRK) and the Department of Water Affairs.

Speakers, who included some of the world's foremost authorities, described how AMD can occur when reactive sulphide minerals are oxidized through exposure to air and water. If sufficient water is present to act as a transport medium and there is not enough alkaline material to neutralize the acid, acidic drainage can result. This is toxic and can pose a serious long-term threat to the environment. Sources of AMD include mining excavations and waste stockpiles but, with suitable know-how, AMD can be prevented, controlled, and/or contained.

Speakers highlighted the need to determine accurately the acid-generation potential of wastes during the planning of a mine, and to establish the level of AMD control required. This is because considerably more technical options are open to proposed mines than to those already generating AMD. Further, the cost of control measures can be included in the financial planning of the mine, providing better control over their economic impact.

Speakers also emphasized the need to determine the length of time that control measures must remain effective, since there are different measures and techniques to provide short- and long-term control of AMD. There are three generally accepted approaches: control of the acid-generation process, control of acid migration, and collection and treatment of AMD. The consensus was that a combination of one or more of these techniques may provide the most secure AMD control.

* Released by Tish Stewart PR Associates, P.O. Box 1683, Parklands 2121.